



Cite this: *Soft Matter*, 2021, 17, 3848

Emergence and stabilization of transient twisted defect structures in confined achiral liquid crystals at a phase transition†

Jose X. Velez,^{‡a} Zhaofei Zheng,^{‡a} Daniel A. Beller^{id}^b and Francesca Serra^{id}^{*a}

Spontaneous emergence of chirality is a pervasive theme in soft matter. We report a transient twist forming in achiral nematic liquid crystals confined to a capillary tube with square cross section. At the smectic–nematic phase transition, intertwined disclination line pairs are observed with both helical and kinked lozenge-like contours, configurations that we promote through capillary cross-section geometry and stabilize using fluorescent amphiphilic molecules. The observed texture is similar to that found in “exotic” materials such as chromonics, but it is here observed in common thermotropic nematics upon heating from the smectic into the nematic phase. Numerical modeling further reveals that the disclinations may possess winding characters that are intermediate between wedge and twist, and that vary along the defect contours. In our experiments, we utilize a phase transition to generate otherwise elusive defect structures in common liquid crystal materials.

Received 16th November 2020,
Accepted 24th March 2021

DOI: 10.1039/d0sm02040k

rsc.li/soft-matter-journal

1 Introduction

In many soft matter and biological systems, a spontaneous emergence of chirality occurs in achiral systems and is responsible for important effects. Chirality can emerge, for example, in spheres confined within a cylinder,¹ in the assembly of rigid rods in a membrane,² in the stacking of disc-like molecules,^{3–7} and in the self-selection of one component in a racemic system.^{8–11} It is hypothesized that a similar mechanism drove the selection of chiral macromolecules in a pre-biotic environment.¹²

In this context, liquid crystal (LC) systems have attracted a great deal of attention as testing grounds for physical principles of emergent chirality. LCs are complex fluids composed of anisotropic molecules, which possess long-range orientational order. Distorting LCs costs elastic energy. In the simplest LC phase, the nematic phase, the bulk elastic energy is given by the sum of the energy penalties due to splay, twist and bend deformations.¹³ Earlier work showed how a twisted configuration is favored if the twist elastic constant is significantly smaller than the other two.^{14,15} More recently, the work of Jeong *et al.* shows how chirality emerges in the equilibrium configuration of an achiral lyotropic chromonic LC droplet

in oil.¹⁶ Here, the twist elastic constant of chromonic LCs is one order of magnitude smaller than the bend elastic constant.¹⁷ The high energy cost of bend in the droplets induces the LCs to twist instead. Similarly, when lyotropic chromonics are confined in round capillary tubes with homeotropic (perpendicular) molecular anchoring on the surface of the capillary, the low twist constant causes the nematic director to twist from the walls to the center of the capillary (twisted escaped radial, or TER, configuration) or to form two intertwined disclination lines (twisted polar, or TP, configuration).¹⁸ More recently, lyotropic micellar LCs and polymeric LCs have been investigated,^{19,20} leading to similar results and showing that the observation of large chiral domains is not uncommon in achiral LC systems whenever twist is energetically cheaper compared to bend and splay.

Achiral thermotropic LCs confined in capillary tubes have been studied extensively.^{21–28} In the smectic-A phase, adjacent LC rods form stacked fluid layers. If a cylinder imposes homeotropic molecular anchoring on its walls, the smectic layers are arranged like the concentric layers of a leek²⁹ in the so-called planar radial (PR) configuration. This can be easily observed with polarized microscopy. When the smectic–nematic phase transition occurs, the system breaks from discrete to continuous translational symmetry, maintaining orientational order. Deep in the nematic phase, LCs experience a frustration in the alignment, which gives rise to two possible configurations: the planar polar (PP) configuration, with two disclination lines running parallel to the side of the capillary, or the escaped radial (ER) configuration, where the LC bends from the walls toward the center of the

^a Johns Hopkins University, Dept. Physics and Astronomy, Baltimore, USA.

E-mail: francesca.serra@jhu.edu

^b University of California, Merced, Dept. Physics, Merced, USA

† Electronic supplementary information (ESI) available. See DOI: 10.1039/d0sm02040k

‡ These authors contributed equally to this work.



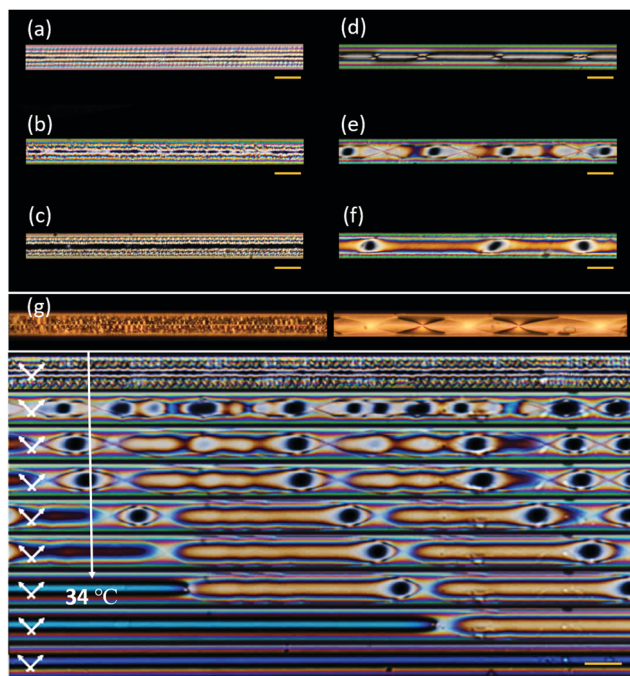


Fig. 1 Polarized microscopy images taken in the smectic-A phase of CCN-47 after cooling from isotropic temperature at different rates: (a) constant cooling at 1 °C min^{-1} , (b) spontaneous cooling after turning off the heating source and (c) quick quenching to room temperature. (d–f) Corresponding configurations at the phase transition. In (d) and (e) there are defect lines, but in (e) the LC is in a double helical structure. In (f) there are no defect lines crossing the capillary. (g) Example of twisted configuration in 8CB, starting from the smectic phase (left) and going into the transient configuration with twisted defect lines at the smectic–nematic transition (right). Bottom: Example of transition from smectic to escaped radial (ER) nematic, going through the transient state with twisted defect lines. Scale bars $50\text{ }\mu\text{m}$.

an example of which is shown in the bottom panel of Fig. 1. Here, heating from 25 °C to 34 °C at a rate of 0.2 °C min^{-1} , we see the twisted configuration. Initially, the onset of the new texture is characterized by the formation of a lozenge-like pattern. At the phase transition (29.4 °C), the smectic defects disappear and the nematic LC adopts a twisted configuration with two defect lines. The structure closely resembles that reported in ref. 18 and 19 for chromonic and lyotropic LCs, respectively, in capillaries with homeotropic anchoring. In our setting, this configuration is transient: eventually, the structure is replaced by an escaped radial (ER) domain, which typically forms at one end of the capillary and expands through the capillary, as shown in Video S1 (ESI[†]). The ER configuration, as seen in ref. 23,25, is stable up until the isotropic phase transition. Notably, when the sample is cooled down into the nematic phase from the isotropic phase, only the (achiral) ER texture is observed. This strongly indicates that the emergence of twist is a consequence of the reorganization that happens at the smectic–nematic phase transition. The twisted defect lines are not exclusive to CCN-47. In fact we observe a similar structure in the common LC 8CB at the smectic–nematic phase transition, as shown in Fig. 1g and in ESI[†] Fig. S2.

While the transient twisted structure can only be observed if the heating rate from smectic to nematic is sufficiently slow, we notice that also the cooling rate from the nematic into the

smectic phase plays an important role. The three different smectic configurations shown in Fig. 1a–c, obtained with different cooling rates, have a different fate when they are then re-heated into the nematic phase. All three configurations show evidence of twist, but the smectic textures obtained with slow or intermediate cooling develop disclination lines (Fig. 1d and e) that cross the capillary at irregular intervals, while for the fastest-quenched LC there are no detectable defect lines crossing the capillary (Fig. 1f). In the case of very slow cooling, the twisted lines are compressed in short segments (Fig. 1d), while the smectic structures quenched at intermediate rate can melt into a smooth double helical structure (Fig. 1e) very similar to the twisted polar (TP) configuration observed in lyotropic LCs.¹⁹ Thus, this system's behavior depends on the cooling rate and the nematic director is influenced by the configuration prior to the phase transition, a possible indication of a memory effect similar to those observed in thin films.⁴⁰

3.3 Twisted defects

To confirm the presence and configuration of the disclination lines, we stabilize them using a CCN-47 and DDAB (0.1%) mixture with BODIPY-C5 fluorophores (Fig. 2a). Following the work by Wang *et al.*,⁴¹ we use amphiphilic fluorescent molecules that self-assemble in disclination lines above a critical

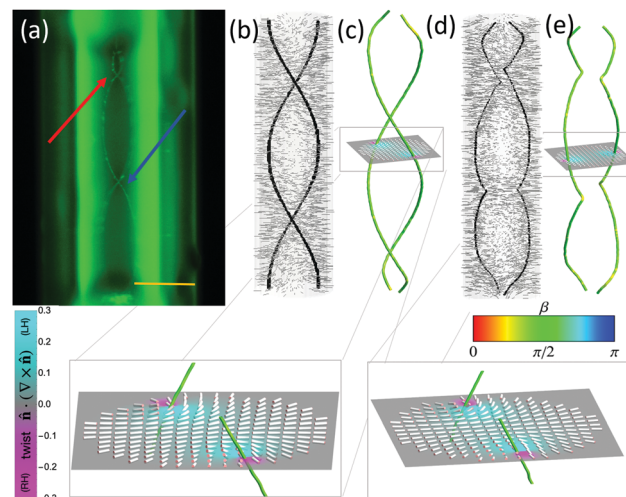


Fig. 2 (a) Fluorescent amphiphile BODIPY-C5 with CCN-47 mixture. Fluorescent molecules accumulate at the defects in the twisting disclination lines. As the escaped radial configuration onsets, the end of the disclination line forms a twisted loop. Scale bar $20\text{ }\mu\text{m}$. (b) and (d) Computer simulated LCs in round capillaries with different elastic anisotropy, forming either a regular helical structure (b) or a lozenge-like structure (d). The elastic anisotropy in (b) is $K_2/K_3 = 0.2$ while in (d) it is $K_2/K_3 = 0.13$. In all cases, $K_1 = K_3 = 10^{-11}\text{ N}$. The simulation size corresponds to a capillary with circular cross section, radius 112.5 nm and length 675 nm . The capillary walls impose strong homeotropic anchoring while the top and bottom are modeled as very weak degenerate planar anchoring. The black lines show the defect lines and the gray glyphs the nematic director. (c) and (e) The twist/wedge character of the twisted defect lines plotted in b and d respectively. The winding type of the disclination is mostly twist (green) but shows an intermediate character (yellow) especially close to the kinks (e). The expanded details show the nematic director on one plane between two twist lines.



concentration. We thus unambiguously confirm the presence of disclinations (Fig. 2a, line indicated by arrows) and we can measure accurately their average distance. In the 50 μm channels, their distance when they appear to intersect while crossing the channel is between 15 and 20 μm . Using the fluorescent amphiphiles is also helpful to stabilize the TP configuration. If the temperature is kept constant very near the phase transition, the twisted configuration persists, and does not turn into an achiral ER configuration for several hours. If the temperature is then increased, the ER structure grows to eventually occupy most of the channel as the defect lines shrink. The defect lines always close into a short-pitched helix (red arrow in Fig. 2a), and shrink until they are coiled into a highly distorted structure that resembles the cord of a landline telephone.

Using Landau-de Gennes numerical modeling of a nematic LC in a cylindrical capillary, we can reproduce the observed double-helix and lozenge-like defect configurations, but only for $K_2 < K_3$ with a ratio below 0.5 (Fig. 2b–d). In particular, the regular twisted structure in Fig. 2b was obtained using a bend and splay constant $K_1 = K_3 = 10^{-11} \text{ N}$ and $K_2/K_3 = 0.2$, while the irregular twist in Fig. 2d was obtained with $K_2/K_3 = 0.13$. For $K_2/K_3 > 0.5$, simulations show an achiral PP configuration as expected. More details on the simulations and the parameters used can be found in ESI.† The size of the simulation (up to hundreds of nanometers) is very different from that of the experiments (tens of microns); therefore in simulations the TP or PP state with two defect lines running along the capillary are always favorable, while in experiment we observe the ER configuration as the stable one. Despite this intrinsic difference, the simulations show many similarities in the shape of the defect lines in the TP state (Fig. 2b and d).

Within the range explored in simulations (*i.e.* smaller than experiments), varying the radius of the capillary does not qualitatively change the behavior, as reported in ESI,† Fig. S3. In addition, we have tested the dependence on the anchoring strength and verified that by reducing the anchoring constant down to 1/20 of its initial value $W_h = 10^{-2} \text{ N m}^{-1}$ does not affect the behavior of the defects, as shown in ESI,† Fig. S4.

The elastic constants used so far are consistent with those utilized to describe other twisted achiral systems such as chromonics and lyotropics. However, we have also numerically modeled the case $K_1 = K_2 < K_3$. The results are reported in ESI,† Fig. S5 and S6, which show the effect of varying the capillary radius/elastic anisotropy and the anchoring constant, respectively. We find once again a qualitative similarity to the experimental observations, with twist emerging and becoming progressively more irregular at higher elastic anisotropy. This indicates that the parameter K_2/K_3 is responsible for the TP configuration, whereas it is not crucial for K_2 to be the smallest elastic constant.

Our numerical findings also highlight a subtlety about the winding character of the disclinations in our system, as compared with recent findings on lyotropic nematics. For the chromonic nematic LCs in a round capillary, a disclination double-helix was reported and suggested to be a twisted planar polar (TPP) state, meaning the director has no component

along the capillary long axis.¹⁸ In contrast, the TP structure observed in a non-chromonic, micellar lyotropic nematic was modeled as a double-helix of twist disclinations, in which a small measuring circuit around either disclination sees the director wind by π about an axis \hat{Q} making a right angle $\beta = \pi/2$ with the local disclination tangent.¹⁹

Neither the TP nor the TPP structure contains wedge disclinations, the $\pm 1/2$ defects familiar from 2D nematic point-defects. In wedge disclinations, a measuring circuit around a disclination sees the director rotate by π about a Frank vector parallel or antiparallel to the local disclination tangent, a situation clearly in contrast to the TPP's twist disclinations, but also impossible in the TP: there, the Frank vector must point along the capillary long axis, which never matches the disclination tangent. Instead, the TPP disclinations have a winding character intermediate between wedge and twist, characterized by an oblique angle β between the Frank vector and the defect tangent.

Does the TP or TPP model describe the disclinations in our system? Both models assume a screw symmetry along the capillary axis, meaning the structure is the same everywhere up to a rotation, consistent with the smooth double-helix defects observed in those works.^{18,19} In contrast, our numerical models, which reproduce the kinked and pinned defect configurations observed in our experiments, indicate that the winding character itself varies along the contour length of each disclination. We observe the following general trends: along segments where the disclination is smoothly undulating and not pinned at an edge, the disclination tends to have twist winding character, or nearly so, consistent with the TP model at a local level (Fig. 2c and e). Twist distortions of both handedness are prominent in the director field on opposite sides of both disclinations, a signature of twist disclinations as noted in ref. 19 (details in Fig. 2c and e). However, near kinks, the winding character becomes somewhat more wedge-like, taking on an intermediate winding character, and kinks are the sites where opposing domains of the spontaneously broken reflection symmetry meet. On one side, the disclinations follow right-handed helices, and the director undergoes right-handed twist in the interior and left-handed twist between the disclinations and the boundary. On the other side of the kink, left-handed and right-handed swap roles in both the director field and the defect contours. (ESI,† Fig. S7).

In certain regions of parameter space, another configuration appears. It is the twisted escaped radial (TER) configuration, observed in chromonics and lyotropic LCs, where the director twists and bends without creating defect lines. Due to the size of the capillary the TP state is always more energetically favorable than the TER configuration, but the latter can be obtained by carefully controlling the initial configuration for the simulation, as detailed in ESI,† Fig. S8. The reason why the size of the simulation is so important is that the diameter of the defect core depends on the molecular size and is therefore not scalable as other length-scales. This was also discussed for LCs near colloidal particles, as detailed in ref. 42.

3.4 The role of edges

In capillaries with a round cross-section, we only rarely observe experimentally the onset of the transient twisted configuration.



- 7 A. M. Sarotti, I. Fernandez, R. A. Spanevello, M. A. Sierra and A. G. Suarez, *Org. Lett.*, 2008, **10**, 3389–3392.
- 8 A. R. Fassihi, *Int. J. Pharm.*, 1993, **92**, 1–14.
- 9 A. N. L. Batista, F. M. dos Santos, J. M. Batista and Q. B. Cass, *Molecules*, 2018, **23**, 492.
- 10 C. P. Brock, W. B. Schweizer and J. D. Dunitz, *J. Am. Chem. Soc.*, 1991, **113**, 9811–9820.
- 11 L. A. Nguyen, H. He and C. Pham-Huy, *Int. J. Biomed. Sci.*, 2006, **2**, 85–100.
- 12 D. G. Blackmond, *Cold Spring Harbor Perspect. Biol.*, 2010, **2**, a002147.
- 13 F. C. Frank, *Discuss. Faraday Soc.*, 1958, **25**, 19–28.
- 14 G. E. Volovik and O. D. Lavrentovich, *Sov. Phys. JETP*, 1983, **58**, 1159.
- 15 R. D. Williams, *J. Phys. A: Math. Gen.*, 1986, **19**, 3211.
- 16 J. Jeong, Z. S. Davidson, P. J. Collings, T. C. Lubensky and A. G. Yodh, *Proc. Natl. Acad. Sci. U. S. A.*, 2014, **111**, 1742–1747.
- 17 E. Romani, A. Ferrarini and C. De Michele, *Macromolecules*, 2018, **51**, 5409–5419.
- 18 J. Jeong, L. Kang, Z. S. Davidson, P. J. Collings, T. C. Lubensky and A. G. Yodh, *Proc. Natl. Acad. Sci. U. S. A.*, 2015, **112**, E1837–E1844.
- 19 C. F. Dietrich, P. Rudquist, K. Lorenz and F. Giesselmann, *Langmuir*, 2017, **33**, 5852.
- 20 C. F. Dietrich, P. Rudquist, P. J. Collings and F. Giesselmann, *Langmuir*, 2021, **37**, 2749–2758.
- 21 D. Melzer and F. R. N. Nabarro, *Philos. Mag. A*, 1977, **35**, 901–906.
- 22 D. Melzer and F. R. N. Nabarro, *Philos. Mag. A*, 1977, **35**, 907–915.
- 23 G. P. Crawford, D. W. Allender and J. W. Doane, *Phys. Rev. A: At., Mol., Opt. Phys.*, 1992, **45**, 8693–8708.
- 24 S. Kralj and S. Z. Žumer, *Phys. Rev. E: Stat. Phys., Plasmas, Fluids, Relat. Interdiscip. Top.*, 1995, **51**, 366–379.
- 25 M. Kleman and O. D. Lavrentovich, *Philos. Mag.*, 2006, **86**, 4117–4137.
- 26 G. De Luca and A. D. Rey, *J. Chem. Phys.*, 2007, **127**, 104902.
- 27 H.-L. Liang, J. Noh, R. Zentel, P. Rudquist and J. P. F. Lagerwall, *Philos. Trans. R. Soc., A*, 2013, **371**, 20120258.
- 28 F. Serra, *Liq. Cryst.*, 2016, **43**, 1920–1936.
- 29 R. Pratibha and N. Madhusudana, *J. Phys. II*, 1992, **2**, 383–400.
- 30 J. Fu, K. Nayani, J. O. Park and M. Srinivasarao, *NPG Asia Mater.*, 2017, **9**, e393.
- 31 K. Nayani, R. Chang, J. Fu, P. W. Ellis, A. Fernandez-Nieves, J. O. Park and M. Srinivasarao, *Nat. Commun.*, 2015, **6**, 8067.
- 32 Z. S. Davidson, L. Kang, J. Jeong, T. Still, P. J. Collings, T. C. Lubensky and A. G. Yodh, *Phys. Rev. E: Stat., Nonlinear, Soft Matter Phys.*, 2015, **91**, 050501.
- 33 L. Tortora and O. D. Lavrentovich, *Proc. Natl. Acad. Sci. U. S. A.*, 2011, **108**, 5163–5168.
- 34 F. Serra, K. C. Vishnubhatla, M. Buscaglia, R. Cerbino, R. Osellame, G. Cerullo and T. Bellini, *Soft Matter*, 2011, **7**, 10945–10950.
- 35 D. V. Sai, T. H. Yoon and S. Dhara, *J. Mol. Liq.*, 2020, **312**, 113410.
- 36 D. A. Beller, *Controlling defects in nematic and smectic liquid crystals through boundary geometry*, PhD thesis, University of Pennsylvania, 2014.
- 37 D. M. Sussman and D. A. Beller, *Front. Phys.*, 2019, **7**, 204.
- 38 G. Duclos, R. Adkins, D. Banerjee, M. Peterson, M. Varghese, I. Kolvin, A. Baskaran, R. Pelcovits, T. Powers, A. Baskaran, F. Toschi, M. Hagan, S. Streichan, V. Vitelli, D. A. Beller and Z. Dogic, *Science*, 2020, **367**, 1120.
- 39 M. C. Choi, T. Pfohl, Z. Wen, Y. Li, M. W. Kim, J. N. Israelachvili and C. R. Safinya, *Proc. Natl. Acad. Sci. U. S. A.*, 2004, **101**, 17340–17344.
- 40 A. Suh, M.-J. Gim, D. A. Beller and D. K. Yoon, *Soft Matter*, 2019, **15**, 5835.
- 41 X. Wang, D. S. Miller, E. Bukusoglu, J. J. de Pablo and N. L. Abbott, *Nat. Mater.*, 2015, **15**, 106–112.
- 42 Y. Luo, D. A. Beller, G. Boniello, F. Serra and K. J. Stebe, *Nat. Commun.*, 2018, **9**, 3841.
- 43 Y. Luo, F. Serra, D. A. Beller, M. Gharbi, N. Li, S. Yang, R. Kamien and K. J. Stebe, *Phys. Rev. E*, 2016, **93**, 032705.
- 44 C. Luo, A. Majumdar and R. Erban, *Phys. Rev. E: Stat., Nonlinear, Soft Matter Phys.*, 2012, **85**, 061702.
- 45 P. G. de Gennes and J. Prost, *The Physics of Liquid Crystals*, Clarendon Press, Oxford, 2nd edn, 1993.
- 46 C. Garland and G. Nounesis, *Phys. Rev. E: Stat. Phys., Plasmas, Fluids, Relat. Interdiscip. Top.*, 1994, **49**, 2964.
- 47 B. Andereck and B. Patton, *Phys. Rev. E: Stat. Phys., Plasmas, Fluids, Relat. Interdiscip. Top.*, 1994, **49**, 1393.
- 48 R. Mahmood, I. Brisbin, C. Gooden, A. Baldwin, D. Johnson and M. Neubert, *Phys. Rev. Lett.*, 1985, **54**, 1031.
- 49 C. Gooden, R. Mahmood, I. Brisbin, A. Baldwin, D. Johnson and M. Neubert, *Phys. Rev. Lett.*, 1985, **54**, 1035.
- 50 H. Hakemi, *Liq. Cryst.*, 1989, **5**, 327.
- 51 S. Srigengan, H. Liu, M. Osipov, R. Mandle, S. Cowling and H. Gleeson, *Liq. Cryst.*, 2020, **47**, 895–907.
- 52 S. Paschel-Schlotthauer, V. Meiwes Turrain, T. Stieger, R. Grotjahn, C. K. Hall, M. G. Mazza and M. Schoen, *J. Chem. Phys.*, 2016, **145**, 164903.
- 53 V. Pergamenschchik, I. Lelidis and V. Uzunova, *Phys. Rev. E: Stat., Nonlinear, Soft Matter Phys.*, 2008, **77**, 041703.
- 54 P. Cladis and S. Torza, *J. Appl. Phys.*, 1975, **46**, 584.
- 55 S. M. Hare, B. Lunsford-Poe, M. Kim and F. Serra, *Materials*, 2020, **13**, 3761.
- 56 D. Svensšek and S. Z. Žumer, *Phys. Rev. E: Stat., Nonlinear, Soft Matter Phys.*, 2004, **70**, 061707.
- 57 L. Lucchetti, G. Nava, R. Barboza, F. Ciciulla and T. Bellini, *J. Mol. Liq.*, 2021, **329**, 115520.

